Cellular/Molecular

An Alternative Exon of CAPS2 Influences Catecholamine Loading into LDCVs of Chromaffin Cells

Olga Ratai,[1] Claudia Schirra,[1] Elvin Rajabov,[2] Irene Brunk,[2] Gudrun Ahnert-Hilger,[2] Praneeth Chitirala,[1] Ute Becherer,[1] David R. Stevens,[1] and Jens Rettig[1]

[1]Department of Cellular Neurophysiology, Center for Integrative Physiology and Molecular Medicine, Saarland University, 66421 Homburg, Germany, and [2]Department of Integrative Anatomy, Charité Universitätsmedizin Berlin, 10117 Berlin, Germany

The calcium-dependent activator proteins for secretion (CAPS) are priming factors for synaptic and large dense-core vesicles (LDCVs), promoting their entry into and stabilizing the release-ready state. A modulatory role of CAPS in catecholamine loading of vesicles has been suggested. Although an influence of CAPS on monoamine transporter function and on vesicle acidification has been reported, a role of CAPS in vesicle loading is disputed. Using expression of naturally occurring splice variants of CAPS2 into chromaffin cells from CAPS1/CAPS2 double-deficient mice of both sexes, we show that an alternative exon of 40 aa is responsible for enhanced catecholamine loading of LDCVs in mouse chromaffin cells. The presence of this exon leads to increased activity of both vesicular monoamine transporters. Deletion of CAPS does not alter acidification of vesicles. Our results establish a splice-variant-dependent modulatory effect of CAPS on catecholamine content in LDCVs.

Key words: **amperometry; chromaffin cells; exocytosis; large dense-core vesicles; priming; readily releasable pool**

Significance Statement

The calcium activator protein for secretion (CAPS) promotes and stabilizes the entry of catecholamine-containing vesicles of the adrenal gland into a release-ready state. Expression of an alternatively spliced exon in CAPS leads to enhanced catecholamine content in chromaffin granules. This exon codes for 40 aa with a high proline content, consistent with an unstructured loop present in the portion of the molecule generally thought to be involved in vesicle priming. CAPS variants containing this exon promote serotonin uptake into Chinese hamster ovary cells expressing either vesicular monoamine transporter. Epigenetic tuning of CAPS variants may allow modulation of endocrine adrenaline and noradrenaline release. This mechanism may extend to monoamine release in central neurons or in the enteric nervous system.

Introduction

The calcium-dependent activator protein for secretion (CAPS aka CADPS) is a cytosolic protein that is required for reconstitution of catecholamine release in cracked PC12 cells (Walent et al., 1992). Experiments performed in PC12 cells, mouse chromaffin cells, and neurons have established that CAPS promotes calcium-dependent regulated fusion of large dense-core vesicles (LDCVs) and synaptic vesicles (for review, see Stevens and Rettig, 2009). CAPS is involved at a prefusion step that regulates releasable pool size in neurons and chromaffin cells by promoting and stabilizing vesicle priming (Jockusch et al., 2007; Liu et al., 2008, 2010). In contrast to the priming factor Munc13, which primes vesicles exclusively by interacting with syntaxin via the Munc13 homology domain (MHD), the priming function of CAPS is not only mediated by its SNARE binding (Khodthong et al., 2011; Kabachinski et al., 2014, 2016), but also by its pleckstrin homology domain (Nguyen Truong et al., 2014). In addition to its priming function, examination of secretion from adrenal chromaffin cells of mice lacking CAPS1 revealed a deficit in catecholamine loading into LDCVs (Speidel et al., 2005). Although this result was disputed immediately (Fujita et al., 2007), an influence of CAPS on monoamine transport by both vesicular monoamine transporter 1 (VMAT1) and VMAT2 has been reported (Brunk et al., 2009).

Two paralogs of CAPS (CAPS1 and CAPS2) are present in mammals and both promote vesicular monoamine uptake by the vesicular monoamine transporters VMAT1 and VMAT2 (Brunk

Received Aug. 9, 2018; revised Oct. 1, 2018; accepted Oct. 27, 2018.

Author contributions: G.A.-H. and J.R. edited the paper; D.R.S. wrote the first draft of the paper. G.A.-H., D.R.S., and J.R. designed research; O.R., C.S., E.R., I.B., P.C., and U.B. performed research; O.R. and C.S. analyzed data.

This work was supported by the Deutsche Forschungsgemeinschaft (Grants SFB 894 and IRTG 1830). We thank Margarete Klose, Anja Ludes, Tamara Paul, Nicole Rothgerber, and Katrin Sandmeier for excellent technical assistance.

The authors declare no competing financial interests.

Correspondence should be addressed to Jens Rettig, Center for Integrative Physiology and Molecular Medicine (CIPMM), Saarland University, Building 48, 66421 Homburg, Germany. E-mail: jrettig@uks.eu.

https://doi.org/10.1523/JNEUROSCI.2040-18.2018

 0270-6474/19/390018-10$15.00/0

et al., 2009), providing a potential mechanism for modulation of catecholamine content of LDCVs. Although CAPS1 knock-down was reported to have no influence on peptide or catecholamine loading in secretory granules in PC12 cells (Fujita et al., 2007), CAPS1 knock-down using an shRNA approach results in a deficit in cargo release from LDCVs (in this case BDNF) in cultured hippocampal neurons (Eckenstaler et al., 2016). The luminal pH of secretory granules located in the dendrites of these cells was increased following knock-down of CAPS, although the decreased cargo release appeared unrelated to the higher pH values. Catecholamine transport via VMATs is ATP dependent and relies on a proton gradient (Johnson, 1988; Forgac, 1989; Henry et al., 1998). Either depletion of the pH gradient or reduction of monoamine transporter function could reduce granule catecholamine content.

In mouse chromaffin cells, deletion of both CAPS genes results in a reduction of the readily releasable pool and of sustained release, resulting in an ~50% reduction in calcium-stimulated secretion (Liu et al., 2008, 2010). We have examined the rescue of catecholamine release following expression of CAPS2 splice variants in mouse chromaffin cells lacking both CAPS genes (double knock-out, DKO) to identify the amino acid sequences involved in modulation of granule filling. We show that the presence of an exon of 40 aa length in CAPS2 is required for both the enhancement of catecholamine content and release observed following introduction of CAPS2 splice variants in mouse DKO chromaffin cells and the enhancement of serotonin (5-HT) uptake following expression of CAPS2 splice variants in Chinese hamster ovary (CHO) cells stably expressing VMAT.

Materials and Methods

Chromaffin cell preparation and infection. CAPS1/CAPS2 DKO mice were generated by breeding the CAPS1 mutation into the CAPS2 knock-out background, as has been described previously. Genotypes were confirmed by PCR using primers described previously (Speidel et al., 2005; Jockusch et al., 2007; Liu et al., 2008). All electrophysiological experiments were performed on chromaffin cells in primary culture derived from mice of either sex. The mice were prepared after hysterectomy on embryonic day 18 (E18) or E19. The preparation of the cells was performed as described previously (Liu et al., 2008). For the CAPS2 splice-variant rescue experiments, isolated chromaffin cells were infected with 70 μl of pSFV1-CAPS2a-IRES-eGFP, pSFV1-CAPS2b-IRESeGFP, and pSFV1-CAPS2c-IRES-eGFP (sequences are from mouse) using methods described previously (Ashery et al., 1999).

Patch-clamp analysis. Conventional whole-cell recordings were performed with 4–6 MΩ pipettes and an EPC-9 patch-clamp amplifier together with Pulse software (HEKA). For measurements from primary chromaffin cells in culture, the extracellular solution contained the following (in mM): 145 NaCl, 2.4 KCl, 10 HEPES, 4.0 $MgCl_2$, 1.0 $CaCl_2$, 10 glucose, pH 7.4, for UV flash experiments (see Fig. 1). For all other experiments, including live-cell imaging, the calcium concentration was raised to 2.5 Ca^{2+} and the Mg^{2+} concentration was 1.5 mM. The intracellular solution for UV flash experiments contained the following (in mM): 100 Cs-glutamate, 2 Mg-ATP, 0.3 Na_2-GTP, 40 Cs-HEPES, 5 nitrophenyl-EGTA (NP-EGTA), 4 $CaCl_2$, 0.4 Furaptra, and 0.4 Fura-4F, pH 7.2. For the single-spike analysis (see Fig. 2), the patch pipette solution contained the following (in mM): 110 L-glutamic acid, 9 H-EDTA, 5 $CaCl_2$, 40 HEPES, 2 Mg-ATP, 0.3 Na-GTP, pH 7.2 and osmolarity of 290 mOsm. Capacitance measurements were performed using the Lindau–Neher technique implemented as the 'sine+dc' mode of the 'software lock-in' extension of PULSE software. A 1 kHz, 70 mV peak-to-peak sinusoid stimulus was applied about a DC holding potential of −70 mV. All experiments were performed at room temperature on cells after 2 d in culture 5–6 h after virus infection. Data are shown as mean ± SEM. We used the Wilcoxon–Mann–Whitney test for comparison of differences between groups. Curve fits were done using IGOR Pro software (Wavemetrics).

Amperometric recordings of catecholamines. Amperometric recordings from isolated chromaffin cells were performed as described previously (Bruns et al., 2000). Carbon fiber electrodes used for amperometry were produced as follows. Carbon fibers (5 μm diameter) were glued to copper cannulae using a conducting carbon paste (Electrodag 5513, Bavaria Elektronik) and then glued inside a glass pipette. The pipettes were then pulled with a conventional puller. The carbon fiber extending beyond the pulled pipette tip was coated with a cathodal paint by electrolysis (2934788, BASF). The assembly was then baked for 20 min at 50°C. The junction between the fiber and the glass was sealed with Sylgard and baked again at 50°C. Before use, the carbon fibers were broken off to expose the tip for recording.

The electrode was connected to the head stage of an EPC7 patch-clamp amplifier (HEKA) and a holding potential of +800 mV was applied in the voltage-clamp mode. Carbon fibers were cut and tested for sensitivity before use and were changed after 2–3 recordings. After the whole-cell configuration was achieved, the carbon fiber was positioned so that it lightly touched the cell that was being recorded. Catecholamines contacting the carbon fiber were immediately oxidized, producing a current on the pipette that was countered by the voltage clamp, allowing recording of catecholamine release as a measure of the amperometric current. For single-spike analysis, the sensitivity of the electrodes to 50 μM adrenaline was tested before use. The analysis was performed with a macro written in the Igor programming language (Wavemetrics). Single events were recognized automatically with a threshold of 5 pA and were then checked visually. The statistic and measurements were then collected using the automated macro.

Preparation of cells for high-pressure freezing. Acutely dissociated chromaffin cells from WT mice and CAPS DKO mice (E18–E19) were plated on collagen-coated sapphire discs (Leica) in four-well plates and cultured at 37°C with 13% CO_2. After 2 d in culture, some wells of CAPS DKO chromaffin cells were infected with 50 μl of activated pSFV1-CAPS2b-IRES-GFP for 5.5–6 h or pSFV-GFP for 3.5–4 h. Sapphire discs with cultured cells were transferred into flat specimen carriers and high-pressure frozen after the addition of DMEM with 30% FCS (EM PACT2, Leica). Untreated control WT and CAPS DKO cells were frozen at the same time.

Freeze substitution, embedding, and cell analysis for postembedding correlative light and electron microscopy (CLEM). Freeze substitution and embedding in Lowicryl was done as described previously (Matti et al., 2013) for postembedding CLEM. Briefly, all samples were further processed in an automatic freeze-substitution apparatus (AFS2, Leica). The temperature was increased from −130 to −90°C for 2 h. Cryosubstitution was performed at −90 to −70°C for 20 h in anhydrous acetone and at −70 to −60°C for 20 h with 0.3% (w/v) uranyl acetate in anhydrous acetone. At −60°C, the samples were infiltrated with increased concentrations (30%, 60%, and 100%; 1 h each) of Lowicryl (3:1 K11M/HM20 mixture with 0.3% uranyl acetate). After 5 h of 100% Lowicryl infiltration, samples were UV polymerized at −60°C for 24 h and for an additional 15 h while raising the temperature linearly to 5°C. Until further processing, the samples were kept in the dark at 4°C. After removing the sapphire discs, two to three 70 nm ultrathin sections were cut parallel to the surface serially, followed by a 400-nm-thick section using a Leica EM UC7. The 70 nm ultrathin sections were collected on pioloform-coated copper grids, stained with uranyl acetate and lead citrate, and analyzed with a Tecnai 12 Biotwin electron microscope (FEI/Philips). The 400 nm section was air-dried on a glass slide for 1 h in the dark and later coverslipped with mounting medium and used within 24 h for structured-illumination microscopy to avoid loss of fluorescence signals in the sections. Several consecutive 70 and 400 nm sections could be cut from the same block face.

The 400 nm sections were imaged using the ELYRA PS.1 superresolution microscope (Carl Zeiss). Images were acquired in the wide-field mode using the 63× Plan-Apochromat (numerical aperture 1.4) objective with excitation light of 488 nm wavelength to identify infected chromaffin cells. First, an overview bright-field image of the cells for cell orientation images was generated. After adjusting the highest and lowest

focus planes for *z*-stack analysis, 1–4 images (488 nm) were recorded with a step size of 0.5 μm to scan the cells of interest. Infected cells were distinguished from uninfected cells by comparison of the fluorescent signals with the surrounding cells or cell clusters. To relocate infected cells, the relative positions of the surrounding cells were used as landmarks in the electron micrograph of the consecutive ultrathin section during electron microscopy (EM) analysis.

2D-EM analysis of chromaffin cells. Electron micrographs (1376 × 1032 pixels) were acquired with a CCD camera (MegaViewIII/Olympus) at 23,000-fold magnification using the multiple image acquisition and alignment iTEM software (version 5.0, Olympus Soft Imaging Solutions). Only cells with a visible nucleus and preserved plasma membrane were analyzed. LDCVs were recognized by their round, dense core. An outline of both the plasma membrane and the nucleus was generated manually and vesicles were marked manually and outlined with a circle. The radius of the vesicle and the shortest distance from its center to the plasma membrane were calculated using software written in house (Liu et al., 2008).

Measurement of 5-HT uptake in CHO cells. The measurement of 5-HT from CHO cells stably transfected with VMAT has been described previously (Brunk et al., 2006, 2009). To directly address VMAT activity, the plasma membrane was disrupted by streptolysin O (SLO) a bacterial cytolysin. CHO cells were incubated at 4°C with SLO, allowing for binding to the plasma membrane. When the temperature was elevated to 25°C, SLO molecules oligomerize, thereby forming pores that allow exchange of the intracellular milieu for a buffer of defined ionic composition. To start uptake, cells were resuspended in a buffer containing the following (in mM): 150 potassium glutamate, 20 PIPES, 4 EGTA, 1 $MgCl_2$, and 1 dithiothreitol, adjusted to pH 7.0 with KOH and 5-hydroxy-[^{3}H]tryptamine trifluoroacetate (5-HT or serotonin; specific activity, 4.33 TBq/mmol, GE Healthcare, 40 nM plus 360 nM unlabeled serotonin) supplemented with or without reserpine (2 μM). Specificity of uptake was estimated by subtracting the unspecific uptake in the presence of reserpine (Brunk et al., 2009).

ClopHensorN(Q69M). ClopHensorN(Q69M) is a fusion protein combining E^{2}GFP and tdTomato (tandem Tomato) via a 20 aa linker (Arosio et al., 2010). E^{2}GFP is generated from EGFP by mutating threonine 203 to tyrosine, which generates an anion-binding site that renders the fluorescence Cl sensitive. We added a further mutation (Q69M) (Griesbeck et al., 2001). To direct ClpH to LDCVs, it was subcloned into a pMax vector containing NPY. We expressed NPY-ClpH into cultured mouse chromaffin cells via electroporation.

ClopHensorN was cut from pBJ1-ClopHensorN (Addgene) using HindIII, treated with Klenow to obtain blunt ends, and then cut with NotI. The plasmid pMax was cut first with EcoRI, treated with Klenow to obtain blunt ends, and then cut with NotI. Both fragments were ligated with T4-ligase to obtain pMax_ClopHensorN.

To introduce the Q69M mutation, E^{2}GFP was amplified in two different PCRs with the following primers: forward: 5′-ATG TAT ACT AGC TAG CTG GAG CCA CCC GCA GTT C-3′; reverse: 5′-TGA AGC ACA TCA CGC CGT-3′ and forward: 5′-ACG GCG TGA TGT GCT TCA-3′; reverse: 5′-ATG TAT ACG AGG ATC CGC GCT TGT ACA GCT CGT CCA T-3′, which were mixed for the last 10 cycles. The E^{2}GFP in pMax-ClopHensorN was replaced by the Q69M mutated E^{2}GFP using the restriction sites NheI and BamHI.

NPY was inserted into pMax_ClopHensorN (Q69M) by PCR using the forward primer (5′-TAT ACC ATC GAT GCG CCA CCA TGC TAG GTA ACA AG-3′) and the reverse primer (5′-ATG TAT ACT AGC TAG CCC ACA TTG CAG GGT CTT C-3′). The PCR product and pMax_ClopHensorN (Q69M) were cut with NheI und ClaI in CutSmart-Buffer at 37°C. Ligation was performed with T4-Ligase at RT for 2 h. NPY und ClopHensor are connected by the Strep-TagII (WSHPQFEK).

Electroporation of mouse chromaffin cells. The preparation of mouse chromaffin cells was performed as described previously. After trituration, the cells were centrifuged in DMEM for 5 min (4000 rpm at room temperature, RT), washed in PBS, and recentrifuged. Electroporation was performed using the Neon Kit (4 glands per six well plate, Invitrogen, catalog #MPK1096) with 4 μg of DNA and electroporated (one pulse at 1400 V for 20 ms) according to the kit instructions. The cells were then diluted to 300 μl with DMEM without penicillin/streptomycin (pen/strep), plated on coverslips, and allowed to adhere in the incubator (37°C, 13% CO_2) for 30 min, after which 3 ml of DMEM with pen/strep was added to each well.

Immunocytochemistry. To confirm that NPY-ClpH was sorted to LDCVs, mouse chromaffin cells were electroporated with pMax-NPY-ClpH and processed after 48 h for immunolabeling. In brief, cells were washed with PBS and then fixed in 4% PFA in PBS at pH 7.4 for 20 min. After several wash steps in PBS, the cells were quenched with 50 mM glycine in PBS for 10 min. The cells were then permeabilized and blocked with 0.1% Triton X-100/2.5% NGS for 30 min. After washing twice with PBS, the cells were incubated with primary antibody (1:100, rabbit anti-chromogranin A; Abcam) overnight at 4°C and with the secondary antibody (1:2000, Alexa Fluor-647-conjugated goat anti-rabbit; Invitrogen) for 1 h at RT. After washing, cells were mounted for imaging.

Images were acquired using an Elyra S1 (Leica) laser-scanning microscope (633 nm, 10% laser intensity, emission filter 638–755 nm, using the Zen program). Sixteen-bit images were acquired using a 63× oil objective (Plan-Apochromat 63×/1.4 Oil DIC M27). E^{2}GFP images were acquired with excitation at 488 nm (12% laser intensity, emission filter 493–533 nm). The images were analyzed using ImageJ to determine the degree of colocalization.

Live-cell imaging. Imaging was performed using the Leica Elyra S1 and images were acquired using Zen software. MCCs were examined 48 h after electroporation with NPY-ClpH. Illumination of E^{2}GFP at 488 nm produces a robust, pH-dependent fluorescence, whereas illumination at 458 nm produces a pH-insensitive fluorescence. Because the fluorescence at 458 nm is relatively weak even at ambient pH, we used illumination at 561, which activates the td-Tomato fluorescence to identify granules. We performed ratiometric measurements using the wavelengths 488 and 458 nm. For ratiometric pH determinations, granules in a 1 μm slice at the footprint of cells were imaged to increase the likelihood that the granules were mature. For pH steps, granules in a 1 μm deep slice at the center of the cell were imaged with illumination at 488 nm and emission at 493–533 nm.

pH calibration. A pH calibration curve was generated using the ratio of the fluorescence with illumination at 488 nm to that at 458 nm of the E^{2}GFP moiety of ClpH. The DMEM solution was removed and replaced with extracellular solution and the cells were located under the microscope. The extracellular solution was then replaced with a pH-clamping solution. Solutions with pH values of 4, 5, 6, 7, 8, and 9 were made as follows. The base solution contained the following (in mM): 30 NaCl, 100 KCl, 2 $MgCl_2$, and 10 glucose, as well as 10 μM nigericin, 4 μM valinomycin, and 5 μM CCCP. Depending on the target pH, lactate (20 mM, pH 4), MES (20 mM, pH 5 and pH 6), or HEPES (20 mM, pH 7–9) were included. After allowing equilibration of the intragranular pH (>5 min), the images were acquired with sequential illumination at 488 nm, 458, and 561 nm. Only granules that were visible in all three images were used for the ratiometric calibration. Ratios of fluorescence vs pH values were fit using a single binding site Hill model in Igor Pro (Wavemetrics). For pH measurements, the coverslips were placed in the observation chamber, filled with extracellular solution, and imaged at room temperature. Images were acquired at 488, 458, and 561 nm. Ratios of fluorescence at 488 and 458 nm were calculated and the pH was interpolated from the calibration-curve fit.

Experimental design and statistical analysis. The data from patch-clamp experiments are shown as averaged curves and presented as mean ± SEM. Because both amperometric and capacitance data are often not normally distributed, the nonparametric Wilcoxon–Mann–Whitney two-sample rank test (as implemented in the statistics package of Igor Pro) was used for tests of significance. Calculated *p*-values are provided when >0.001. For *p*-values <0.001, $p < 0.001$ is indicated rather than the calculated *p*. Comparisons are between CAPS DKO chromaffin cells and CAPS DKO chromaffin cells expressing the splice variant of interest from the same mouse or DKO littermates. The Wilcoxon rank test was also used to test for significance of differences in the uptake of 5-HT into CHO cells expressing VMATs. Colocalization was quantified using ImageJ.

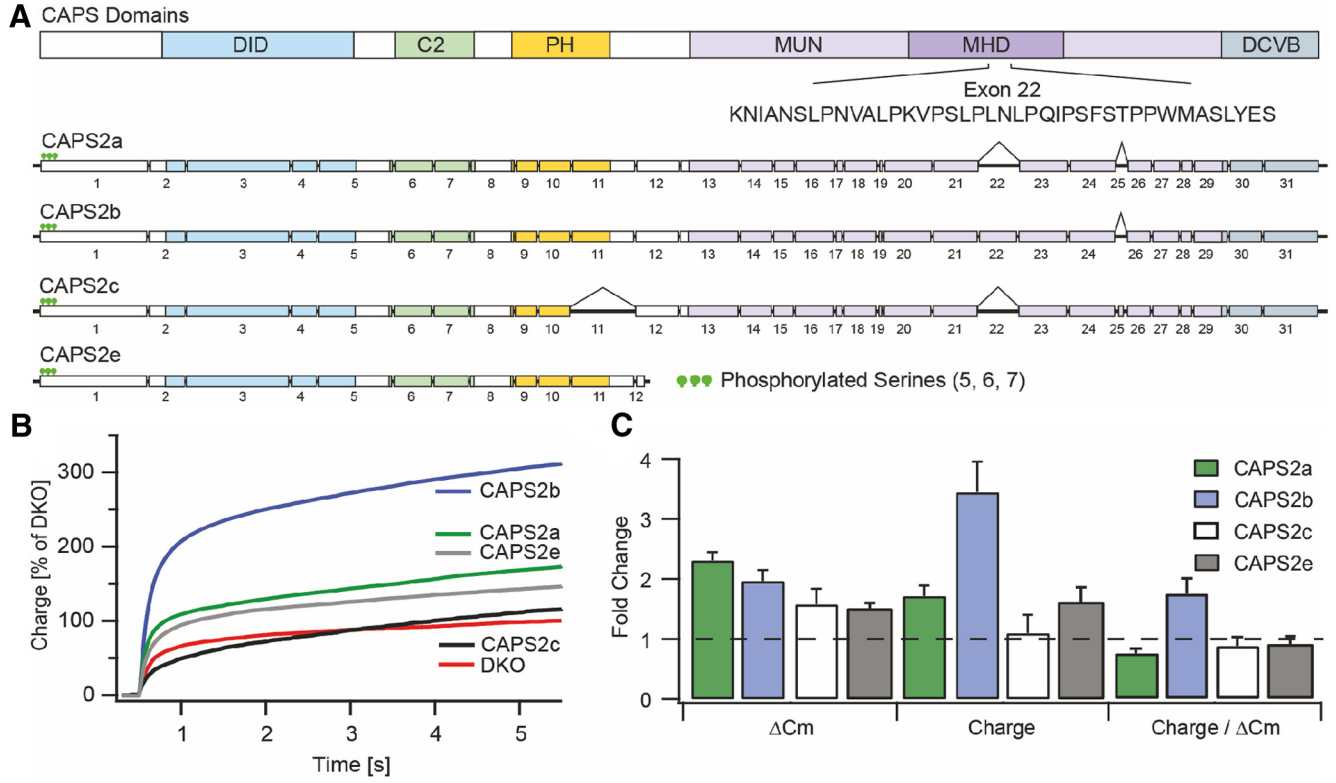

Figure 1. CAPS2b modulates catecholamine content of LDCVs. ***A***, Suggested domain structure of the CAPS2 gene. Proven domains are color coded (top). Exon composition of the four splice variants (CAPS2a, CAPS2b, CAPS2c, and CAPS2e) are shown in the bottom. ***B***, Cumulative charge (integral of amperometric responses) relative to the mean DKO responses of CAPS2 splice variants expressed in CAPS DKO chromaffin cells DKO, $N = 4, n = 20$; CAPS2a, $N = 5, n = 26$; CAPS2b, $N = 5, n = 27$; CAPS2c, $N = 4, n = 17$, CAPS2e, $N = 4, n = 14$ where N is the number of mice and n is the number of cells. ***C***, Relative (fold change vs DKO) of capacitance changes (ΔC_m) and amperometic charge, as well as the relative (fold change) ratio of amperometric charge/capacitance change are shown for CAPS2a (green)-, CAPS2b (blue)-, CAPS2c (white)-, and CAPS2e (gray)-expressing DKO chromaffin cells. Capacitance data are taken from Nguyen Truong et al. (2014).

Results

Exon 22 of CAPS2 modulates LDCV catecholamine release

Expression of four of the six CAPS2 splice variants described by Sadakata et al. (2007a) reversed, to varying degrees, the deficit in priming observed after knock-out of both CAPS genes (DKO) (Nguyen Truong et al., 2014). Figure 1*A* shows the domain structure of CAPS2 and the exon structure of the four splice variants that, when expressed, significantly increased secretory responses in CAPS DKO chromaffin cells. Of the four splice variants examined, CAPS2a, CAPS2b, and CAPS2c contain all domains. CAPS2e is truncated shortly after the pleckstrin homology domain and lacks the MUN and MHD domains and the C-terminal end. CAPS2c lacks exon11, resulting in truncation of the centrally located pleckstrin homology domain that has been implicated in plasma membrane association (Kabachinski et al., 2014) and in priming (Nguyen Truong et al., 2014). In addition, CAPS2c contains exon 25, encoding 5 aa in the C-terminal end of the MUN domain. The MUN domain, which includes an MHD, is involved in the priming function of CAPS via an interaction with SNARE complexes (James et al., 2009, 2010; Daily et al., 2010; Khodthong et al., 2011; Kabachinski et al., 2014). In contrast, CAPS2a and CAPS2b both lack exon 25 and differ only in exon 22 that is absent in CAPS2a and present in CAPS2b.

To identify potential domains involved in catecholamine loading, we compared catecholamine release measured using carbon fiber amperometry with the exocytosis as indicated by membrane capacitance (C_m) increases (recorded from the same cells). The membrane capacitance data of this dataset were reported previously (Nguyen Truong et al., 2014). Figure 1*B* shows catecholamine release following expression of CAPS2a, CAPS2b, CAPS2c, and CAPS2e, respectively, in chromaffin cells derived from CAPS DKO mice. Each of the constructs that produced an enhancement of secretion was detectable by Western blot as a single band of the expected molecular mass after expression (Nguyen Truong et al., 2014). The cumulative catecholamine release based on the integral of carbon fiber amperometric measurements revealed a large difference in ability of the four splice variants to enhance catecholamine release. Secretion was triggered by UV flash photolysis of calcium-loaded NP-EGTA that was included in the patch pipette. The mean responses are presented as change relative to DKO controls. Although CAPS2b expression increased the charge ~3-fold (345 ± 46.2%, $p < 0.001$) compared with DKO cells, the increase upon CAPS2a expression was more moderate (172 ± 18.3%, $p < 0.001$). CAPS2c expression did not lead to an increase in charge (113 ± 31.3%), whereas CAPS2e produced an increase similar to that produced by CAPS2a expression (162 ± 24%, $p = 0.004$).

The large difference in catecholamine release between CAPS2a- and CAPS2b-expressing cells [Fig. 1*B*, charge (mean fold change ± SEM)] is in stark contrast to the differences in the C_m measurements (mean fold change ± SEM), which showed a similar CAPS2a and CAPS2b rescue (ΔC_m, Fig. 2-1, available at https://doi.org/10.1523/JNEUROSCI.2040-18.2018.f2-1, and Nguyen Truong et al., 2014). Figure 1*C* shows a summary of the fold change in C_m relative to the DKO control (derived from Nguyen Truong et al., 2014). Also shown is the fold change in amperometric response (charge) relative to the DKO control and the fold change in charge/fold change in C_m for each splice variant. Al-

though each of these constructs enhances exocytosis in CAPS DKO cells, only expression of CAPS2b produced a significant enhancement of the quotient of the charge divided by C_m ((1.75 ± 0.16, $p <$ 0.001) for CAPS2b versus 0.76 ± 0.11, 0.72 ± 0.09, and 0.92 ± 0.13 for CAPS2a, CAPS2c, and CAPS2e, respectively). Because CAPS2a and CAPS2b differ only in exon 22, a proline-rich 40 aa stretch within the Munc13 homology domain, these data indicate that the presence of this amino acid sequence influences the catecholamine content of chromaffin granules.

To confirm this result and to investigate how expression of exon 22 enhances catecholamine release, we characterized the parameters of individual amperometric events caused by the fusion of single LDCVs (Wightman et al., 1991) following expression of CAPS2a and CAPS2b in CAPS DKO cells. The capacitance changes were measured in the whole-cell patch-clamp configuration (Fig. 2*A*). The recording pipette solution contained a free $[Ca^{2+}]_i$ of ~6 μM, which induced secretion at a low frequency, allowing discrimination of single-granule fusion events. After achieving the whole-cell recording mode, amperometric signals and whole-cell capacitance were recorded for 3 min. In agreement with our previously published data (Nguyen Truong et al., 2014) and the results above, CAPS2a and CAPS2b expression produced a robust increase in membrane capacitance compared with DKO chromaffin cells (Fig. 2*A*,*B*).

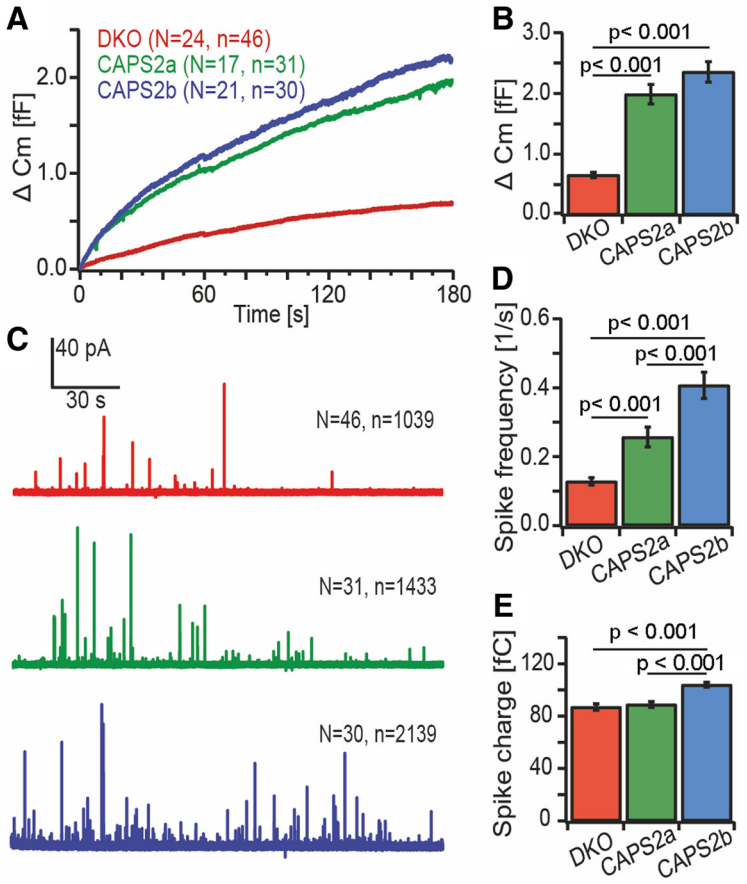

Figure 2. Exon 22 of CAPS2 modulates LDCV catecholamine release. ***A***, Responses of E19 mouse chromaffin cells to perfusion with 6 μM $[Ca^{2+}]_i$. The averaged capacitance responses measured in CAPS DKO cells (red) and in DKO cells expressing either CAPS2a (green) or CAPS2b (blue) are shown. *N* = number of mice, *n* = number of cells. ***B***, Mean C_m change (mean ± SEM) of each treatment group. ***C***, Representative amperometric traces recorded during the capacitance measurements shown in ***A***. *N* = number of cells, *n* = number of spikes. ***D***, Frequency histograms of amperometric spikes observed in CAPS DKO cells and in CAPS DKO cells expressing either CAPS2a or CAPS2b (mean ± SEM). ***E***, Histograms of mean single-spike charge observed in CAPS DKO cells and in CAPS DKO cells expressing either CAPS2a or CAPS 2b. Statistical significance was determined using Wilcoxon–Mann–Whitney test. See Figure 2-1 (available at https://doi.org/10.1523/JNEUROSCI.2040-18.2018.f2-1) for amperometric spike distribution in DKO and CAPS2a- and CAPS2b-expressing DKO cells.

The representative traces of the amperometric responses reflect the much lower frequency of events in the DKO cells and mirrored the reduced capacitance responses observed in these cells (Fig. 2*C*). Although expression of both CAPS2a and CAPS2b led to a significant increase in amperometric events ($p < 0.001$), expression of CAPS2b led to a greater increase in event frequency ($p < 0.001$, DKO = 0.13 ± 0.01 Hz; CAPS2a = 0.26 ± 0.03 Hz; CAPS2b = 0.41 ± 0.04 Hz; Fig. 2*D*). This effect can at least partially be explained by a right shift in the amplitude distribution for CAPS2b-expressing cells that moves more events over the detection limit of our carbon fiber (5 pA; Fig. 2-1, available at https://doi.org/10.1523/JNEUROSCI.2040-18.2018.f2-1). We also estimated the charge of individual granules by integrating the single amperometric spikes. Interestingly, the mean charge per spike was also significantly higher in CAPS2b-expressing DKO cells (103.4 ± 1.83 fC) than in DKO cells (87.9 ± 2.4 fC, $p < 0.001$) or CAPS2a-expressing DKO cells (88.9 ± 2.19 fC, $p < 0.001$) cells (Fig. 2*E*). There was a miniscule increase in the spike amplitude (17.32 ± 0.29 pA), rise time of spikes (0.84 ± 0.01 ms), and spike width (4.68 ± 0.049 ms) from CAPS2b-expressing DKO cells as opposed to CAPS2a-expressing DKO cells (15.54 ± 0.31 pA, 0.80 ± 0.02 ms and 4.28 ± 0.059 ms, n.s., respectively). The difference in spike shape is consistent with an increase in catecholamine content of LDCVs in DKO cells expressing CAPS2b. Overall, our amperometric measurements clearly demonstrate that, in addition to promoting LDCV priming, CAPS2b increases the catecholamine content of vesicles whereas CAPS2a promotes only vesicle priming.

CAPS2b overexpression has no influence on LDCV density and LDCV distribution in mouse chromaffin cells

The observed increase in spike frequency in CAPS2b-expressing DKO cells could be due to effects upstream of priming such as increased granule biogenesis, high granule numbers, or to increased docking of granules. We performed EM in WT, CAPS DKO, and CAPS DKO chromaffin cells expressing either CAPS2b or a vector expressing GFP without CAPS to determine whether there are changes in cell morphology or in the size, density, or distribution of LDCVs (Fig. 3). In Figure 3*A*, a representative image of a chromaffin cell is shown on the left with a magnified view of a granule-rich area shown on the right. The insets in the upper right of this image show examples of structures that we included in the analysis (top row). Only granules that possessed a visible lipid bilayer membrane and were electronically denser than mitochondria were analyzed. Analysis of the area of individual chromaffin cells and the areas of the nucleus and the cytosol in

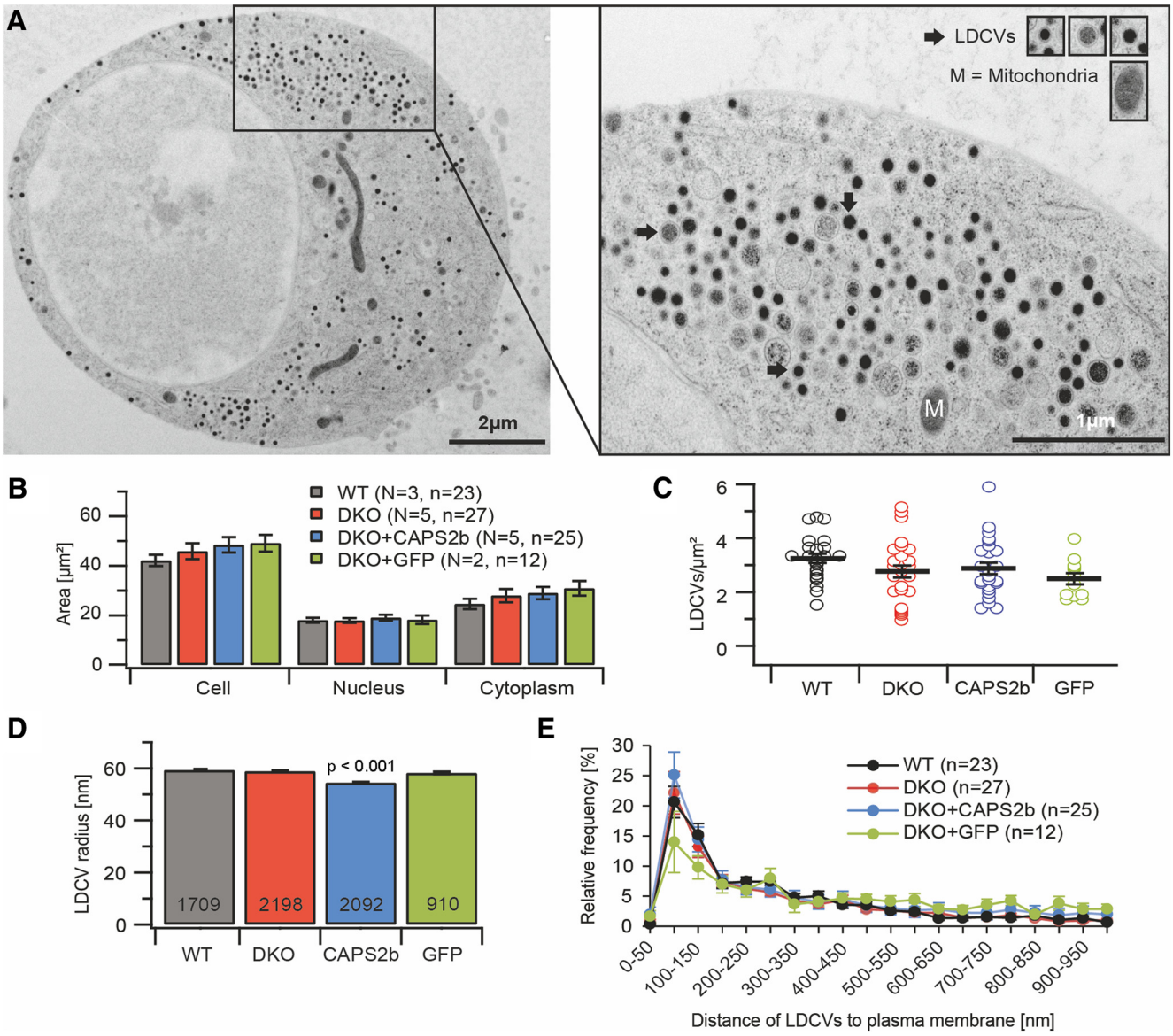

Figure 3. CAPS2b overexpression has no influence on LDCV density and LDCV distribution in mouse chromaffin cells. ***A***, Representative electron micrograph of a chromaffin cell illustrating the analysis method. Black arrows indicate examples of LDCVs that were included in the analysis. ***B***, Quantification of surface area of cell, nucleus, and cytoplasm of four different groups (WT, CAPS1/2-deficient cells (DKO), DKO expressing GFP and DKO expressing CAPS2b) as indicated. N = number of mice, n = number of cells. ***C***, Quantification of LDCVs per area (in square micrometers) for the four different groups. LDCVs were analyzed with the EasyCell program. In all groups, a similar cytoplasmic area was analyzed. ***D***, Analysis of LDCV radius of the four different groups. Statistical significance was determined using Wilcoxon–Mann–Whitney test ($p < 0.001$). n = number of LDCVs. ***E***, Distribution of LDCV distances from the plasma membrane quantified for the four different groups. n = number of cells.

WT cells, DKO cells, and DKO cells expressing CAPS2b or GFP revealed similar values for all groups (Fig. 3*B*). Likewise, the distribution of LDCV density was indistinguishable in these four groups of cells (Fig. 3*C*). Importantly, there was no significant difference in LDCV density or cell area between DKO and CAPS2b-expressing or GFP-expressing DKO cells, indicating that changes due to CAPS2 splice variant expression are not the result of viral infection. The mean granule radius in CAPS2b-expressing DKO cells was smaller (DKO = 58.94 ± 0.41; GFP = 58.27 ± 0.50; WT = 59.36 ± 0.38; CAPS2b = 54.50 ± 0.31 nm, $p < 0.001$) than that observed in the other cells (Fig. 3*D*). Finally, we also examined the distribution of LDCVs with respect to the distance from the plasma membrane. Figure 3*E* shows the relative frequencies of LDCVs at different distances from the PM, which were also similar for DKO, CAPS2a, and CAPS2b, although there appears to be a reduction of granules near the membrane after expression of the GFP control vector in DKO cells. In conclusion, our EM studies show that the enhanced granule fusion and content following expression of CAPS2b is not due to effects on biogenesis or distribution of chromaffin granules.

LDCVs from CAPS DKO chromaffin cells have a similar pH as LDCVs from WT chromaffin cells

To test whether the previously reported differences in pH (Eckenstaler et al., 2016) are responsible for differences in catecholamine content, we compared the pH of LDCVs in WT chromaffin cells with those of CAPS DKO chromaffin cells. To this end, we performed ratiometric measurements of pH with ClopHensorN, a fusion protein of E^{2}GFP and td-Tomato. ClopHensorN has been used previously for ratiometric measure-

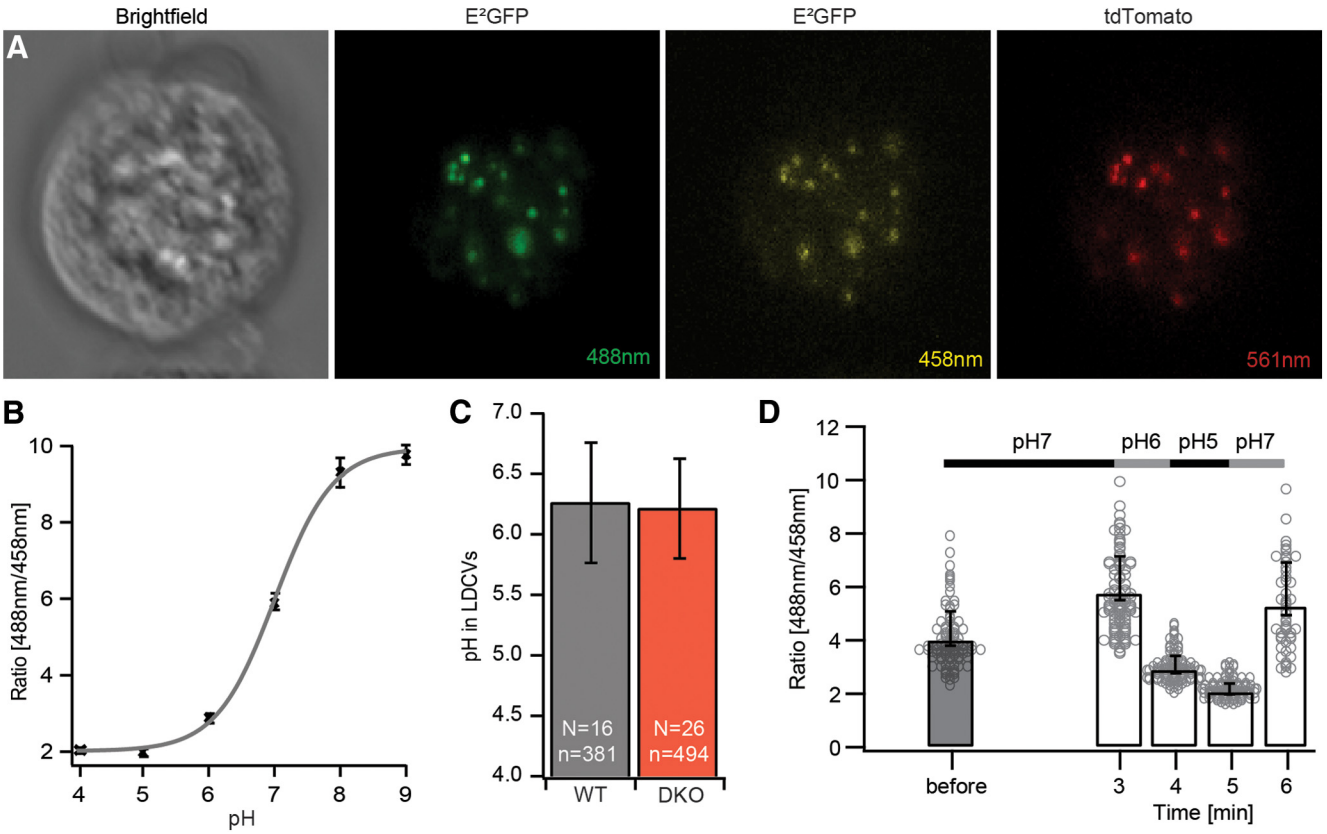

Figure 4. LDCVs from CAPS DKO chromaffin cells have a similar pH as LDCVs from WT chromaffin cells. ***A***, Left to right, Bright-field image of a live chromaffin cell transfected with NPY-ClpH; fluorescent image excited at 488 nm to visualize E^{2}GFP at its pH-dependent wavelength; fluorescent image excited at 458 nm to visualize E^{2}GFP at its isosbestic point; and fluorescent image excited at 594 nm to visualize td-Tomato. ***B***, pH calibration curve for this ratio. The fluorescence following excitation at 488 nm is pH sensitive, rendering the ratio of fluorescence at 488 to 458 nm pH sensitive. ***C***, Measured pH in LDCVs in WT and CAPS DKO chromaffin cells. N = number of cells, n = number of granules. ***D***, Clamping the pH of chromaffin cells from CAPS DKO cells expressing NPY-ClpH. Shown are the ratios ± SEM of the granule fluorescence at ambient pH ($n = 93$, $N = 8$) and following application of solutions clamping sequentially to pH 7.0 ($n = 93$, $N = 8$), pH 6.0 ($n = 93$, $N = 8$), pH 5.0 ($n = 86$, $N = 7$), and then returning to pH 7 ($n = 50$, $N = 3$). See Figure 4-1 (available at https://doi.org/10.1523/JNEUROSCI.2040-18.2018.f4-1) for localization of NPY-ClpH to chromaffin granules.

ment of intracellular pH and chloride concentration (Arosio et al., 2010). We generated a Q69M ClopHensorN mutant (ClpH) fused to NPY. This mutation increases stability and lowers the pKa (Griesbeck et al., 2001). We established that NPY-ClpH was correctly sorted to LDCVs by expressing NPY-ClpH in chromaffin cells via electroporation (see Materials and Methods) and then staining with an antibody against chromogranin A (a component of the dense core of LDCVs (Machado et al., 2010; Fig. 4-1, available at https://doi.org/10.1523/JNEUROSCI.2040-18.2018.f4-1) after fixation. The NPY-ClpH signal was punctate and to a large degree correlated with that of the chromogranin A signal (Pearson's coefficient = 0.81 ± 0.22, mean ± SEM, Mander's coefficient for NPY-ClpH vs chromogranin A = 0.68 ± 0.25, Mander's coefficient for chromogranin A vs NPY-ClpH = 0.36 ± 0.26), clearly indicating that NPY-ClpH is specifically localized to LDCVs.

After verifying that NPY-ClpH was colocalized with chromogranin A, we performed ratiometric measurements of pH. We measured fluorescence at 502–556 nm following excitation at 488 nm, which causes pH-sensitive excitation, and at 458 nm, which is pH insensitive. The signal at 561 nm was also recorded to visualize td-Tomato (Fig. 4*A*). We generated an *in vivo* calibration curve for NPY-ClpH by clamping mouse E19 chromaffin cells at various pH values (pH 4–9) using the solutions described (see Materials and Methods). The obtained calibration curve was sigmoid with an apparent pK_a of 7.1 (Fig. 4*B*). We performed ratiometric measurements of granule pH in WT and DKO chromaffin cells. The mean estimated pH of granules was 6.22 in WT cells (WT, $n = 381$, 16 cells) and 6.24 in DKO cells ($n = 494$, 26 cells, Fig. 4*C*) and there was no difference between the two groups (Wilcoxon–Mann–Whitney test). This result indicates that the observed difference in granule filling is not pH related. Because this result differs from the observations in hippocampal synapses in cell culture following CAPS knock-down (Eckenstaler et al., 2016), we performed an additional experiment in which we measured the responses of NPY-ClpH-expressing granules to stepwise changes in pH (solutions used were those used to calibrate the pH). In these experiments, the granule pH responded rapidly to changes in pH, stabilizing within 3 min of the solution change. We assessed the fluorescence ratio (488/458 nm) under ambient conditions and then added the clamping solutions sequentially to step the pH to 7.0, followed by steps to pH 6.0, then pH 5.0, and then returned to pH 7.0 (Fig. 4*D*).

Introduction of the pH 7.0 clamping solution produced an increase in fluorescence ratio and introduction of the pH 6.0 solution led to a decrease in ratio beyond the ambient fluorescence ratio before the shift to pH 7.0. Upon introduction of the pH 5.0 solution, further quenching occurred. Return to pH 7.0 led to a return to a similar fluorescence ratio as observed after the first application of the pH 7.0, indicating that the loss of fluorescence in pH 6.0 and pH 5.0 solution was due to pH-dependent quenching and not to bleaching. In all cells, the fluorescence ratio

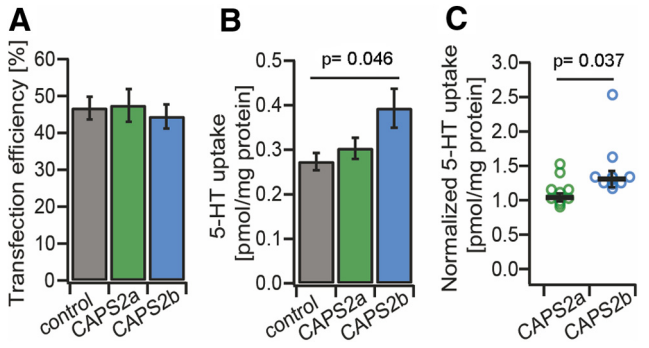

Figure 5. CAPS2b expression, but not CAPS2a expression, increases the uptake of serotonin in CHO cells. ***A***, Transfection efficiency of three different constructs, GFP (control), CAPS2a, and CAPS2b, into CHO cells stably expressing VMAT1. ***B***, Amount of 5-HT uptake into CHO cells transfected with the three different constructs as indicated. 5-HT uptake was significantly higher in cells expressing CAPS2b than in cells expressing either the empty vector or CAPS2a, respectively ($p = 0.046$). ***C***, CHO cells expressing CAPS2b accumulated significantly more 5-HT/mg protein than did CAPS2a expressing cells ($p = 0.037$, $n = 11$).

of granules before the first application of pH 7.0 solution was between the ratio observed at pH 6.0 and pH 7.0, indicating that the granule pH was indeed between 6 and 7. This result indicates that the lower catecholamine content of chromaffin granules in CAPS DKO cells is not the result of a lack of an adequate pH gradient.

CAPS2b expression, but not CAPS2a expression, increases the uptake of serotonin in CHO cells

Our results discount the possibility that lack of granule acidification explains the effects of CAPS2b on catecholamine loading. We next tested whether the uptake of 5-HT by the VMAT is altered upon expression of CAPS2 splice variants. These experiments were performed in CHO cells stably expressing VMAT1, which were transfected with CAPS2a, CAPS2b, or the control vector expressing only GFP. After transfection, cells were permeabilized by SLO following incubation with radioactively labeled serotonin for 15 min, followed by centrifugation and washing (see Materials and Methods). The pellets were then lysed and a protein extraction was performed. Although the transfection efficiency of all three constructs was almost identical (Fig. 5*A*), the amount of serotonin uptake measured per milligram protein was significantly increased in CAPS2b-expressing cells compared with GFP- or CAPS2a-expressing cells (Fig. 5*B*; $^{*}p < 0.05$). Normalization of the single-cell values to the values of GFP-expressing control CHO cells clearly showed that expression of CAPS2b, but not of CAPS2a, resulted in an enhancement of 5-HT uptake (Fig. 5*C*; $^{**}p < 0.01$). Comparable results were obtained with both VMAT1-expressing (Fig. 5) and VMAT2-expressing (data not shown) CHO cells. These results extend the reported enhancement of VMAT activity by CAPS (Brunk et al., 2009) and identify the presence of exon 22 as a requisite for this activity.

Discussion

Here, we present results demonstrating that the modulation of catecholamine filling by CAPS2 requires a short, proline-rich amino acid sequence coded by a single conserved exon. The observation that the ratio of amperometric charge to capacitance change was almost doubled in DKO cells rescued by CAPS2b as opposed to other splice variants, including CAPS2a, strongly supports this conclusion. The comparison of rescue by CAPS2a and CAPS2b is particularly convincing because the presence of exon 22 is the only difference between these two proteins.

The results of the single-spike amperometric analysis also support this conclusion. Although the CAPS2b-expressing cells did exhibit larger capacitance changes, the discrepancy between capacitance measurements and amperometric events in CAPS2a- and CAPS2b-expressing cells cannot be explained by differences in secretion. Despite the finding that CAPS2b granules were slightly smaller, which may indicate less content (Finnegan et al., 1996; Gong et al., 2003), the mean amperometric charge was significantly increased, possibly indicating that CAPS2b produces a modest increase in the concentration of catecholamines in granules. In addition to the shift in spike amplitude distribution shown in Fig. 2-1 (available at https://doi.org/10.1523/JNEUROSCI.2040-18.2018.f2-1), a higher incidence of unfilled granules in the CAPS2a-expressing cells could also contribute to the discrepancy in spike frequency. Approximately 8% of the chromaffin granules in bovine chromaffin cells may be unfilled and these granules undergo fusion (Tabares et al., 2001), but will not produce amperometric events.

Our results are not a consequence of disturbed biogenesis of LDCVs because the density of granules and their distribution in the cytoplasm and at the plasma membrane are similar in DKO, CAPS2b-expressing, and CAPS2a-expressing chromaffin cells. Although the GFP-expressing controls exhibited a decrease in granules adjacent to the plasma membrane, this was not observed in the CAPS constructs containing GFP as an IRES construct. This difference is likely due to a much higher expression of GPP in the GFP control. The results indicate that CAPS protein expressing exon 22 modulates the filling of chromaffin granules via an effect on VMATs.

We have addressed the possibility that the effects of CAPS on granule filling occur as a result of changes in the intragranular pH. Our ratiometric experiments with NPY-ClpH indicate that the intragranular pH of WT and CAPS-DKO cells were virtually identical. Although similar, the pH values we observed are higher than has been reported in the literature (Johnson, 1988; Henry et al., 1998). Although it is conceivable that the pH shift during calibration was not complete or that we have overestimated pH, based on our pH step experiments, we can rule out that the LDCVs in our cells exhibit pH values significantly <6.0, that there is a difference in pH of WT and DKO cells, and that the observed differences in catecholamine filling are a result of differences in intragranular pH.

We directly tested whether expression of exon 22 affects catecholamine uptake by comparing the effects of expression of CAPS2a, CAPS2b, and a vector lacking CAPS on uptake of 5-HT into CHO cells stably transfected with VMAT1. We show that, with similar transfection efficiency, in cells expressing CAPS2b, the catecholamine uptake was significantly higher than that in cells expressing either CAPS2a or only GFP. Therefore, in an unrelated cell type, we also observed an enhancement of catecholamine uptake by VMAT1 that is exon22 dependent. Because this effect appears selective for VMATs, it will affect loading of catecholamines and 5-HT but not amino acid transmitters or peptides. Because CAPS has been reported to function in neuronal priming, it is conceivable that this mechanism will affect neurons of the CNS, vegetative nervous system, and enteric nervous system.

The original study on CAPS function showed that chromaffin granules from embryonic, CAPS1-deficient chromaffin cells had a deficit, not only in amperometric responses relative to capacitance responses, but also in amperometric spikes relative to observation of fusion events using total internal reflection fluorescence (TIRF) microscopy (Speidel et al., 2005). That deficit in

catecholamine loading could be rescued by reintroduction of CAPS1. Later, we showed that CAPS1 could rescue the priming and loading phenotype in CAPS1/CAPS2 DKO chromaffin cells (Liu et al., 2008, 2010) and that CAPS1 promotes catecholamine loading by VMAT1 and VMAT2 to a similar extent as CAPS2 (Brunk et al., 2009). As in CAPS2, CAPS1 also exists in several splice variants. In contrast to CAPS2, however, exon 22 is expressed in all four splice variants reported for CAPS1 in the Ensembl database (Zerbino et al., 2018). Sequence alignment of exon 22 reveals a slight difference in length (49 aa for CAPS1 vs 40 aa for CAPS2b), but a high degree of similarity. In both paralogs, this exon contains a large number of regularly spaced prolines (9 for CAPS1, 8 for CAPS2b), a known helix breaker. Because CAPS1 has been reported to affect granule filling and VMAT activity to a similar degree as CAPS2b, it seems reasonable to assume that exon 22 mediates the modulation of the filling function in CAPS1 as well. Interestingly, all five CAPS splice variants from *C. elegans* lack exon 22, probably explaining why no effect on vesicle filling was reported in CAPS studies from this organism (Speese et al., 2007; Hammarlund et al., 2008; Lin et al., 2010) and suggesting that this modulatory effect was added later in evolution as more complex organisms emerged.

The results presented here can now explain the puzzling observation that only filling, not priming, is affected in embryonic CAPS1-deficient chromaffin cells (Speidel et al., 2005). We could previously show by RT-PCR in E18 adrenal glands that only mRNA from CAPS1 and CAPS2e is detected (Nguyen Truong et al., 2014). At later times of development (postnatal days 1, 10, and 21), mRNA of CAPS1 and all CAPS2 splice variants were traceable. Using a CAPS2b-specific antibody directed against the amino acids of exon 22, we could show that embryonic chromaffin cells indeed do not express CAPS2b (data not shown). Because all experiments in Speidel et al. (2005) were conducted in embryonic chromaffin cells (due to the lethal phenotype of CAPS1 KO), only CAPS2e would be present to compensate for an eventual phenotype of CAPS1 deficiency. We have shown previously that CAPS2e, which as a short splice variant ends after exon 11 and thus also lacks exon 22, is capable to mediate priming of chromaffin granules, explaining the reported lack of a priming deficit in embryonic CAPS1-deficient chromaffin cells (Speidel et al., 2005).

Although our data clarify the controversy about whether CAPS affects vesicle filling and identify the region responsible for this effect, the mechanism of the effect of CAPS on granule filling remains enigmatic. Using TIRF microscopy, we did not observe an increased association of CAPS2b with chromaffin granules compared with CAPS2a (data not shown), ruling out that the effect on filling is mediated by a different localization of the splice variants. Our attempts to identify potential binding partners, probably VMAT itself, by yeast two-hybrid, GST pull-down and peptide-binding assays remained unsuccessful. Even immunoprecipitation experiments with a newly generated antibody specific for exon 22 did not yield any results (data not shown). Potential reasons for this failure could be the transient nature of a potential interaction or incomplete folding of exon 22 due to its high proline content. Alternatively, the proline-rich exon 22 might alter the positioning of other domains in CAPS, thereby allowing the formation of a binding pocket consisting of different regions of CAPS. Regardless of the lack of molecular mechanism, the fact that different splice variants affect not only priming, but also filling, of vesicles in various ways highlights the layer of complexity underlying synaptic transmission. Considering that CAPS has been implicated in diseases such as autism, Alzheimer's disease, Parkinson's disease, and cancer (Sadakata et al., 2007b, 2013; Liu et al., 2011; Vélez et al., 2013; Bonora et al., 2014; Xue et al., 2016; Grabowski et al., 2017; Obergasteiger et al., 2017), an understanding of the function of individual domains of this protein appears worthwhile.

References

Arosio D, Ricci F, Marchetti L, Gualdani R, Albertazzi L, Beltram F (2010) Simultaneous intracellular chloride and pH measurements using a GFP-based sensor. Nat Methods 7:516–518. CrossRef Medline

Ashery U, Betz A, Xu T, Brose N, Rettig J (1999) An efficient method for infection of adrenal chromaffin cells using the semliki forest virus gene expression system. Eur J Cell Biol 78:525–532. CrossRef Medline

Bonora E, Graziano C, Minopoli F, Bacchelli E, Magini P, Diquigiovanni C, Lomartire S, Bianco F, Vargiolu M, Parchi P, Marasco E, Mantovani V, Rampoldi L, Trudu M, Parmeggiani A, Battaglia A, Mazzone L, Tortora G; IMGSAC, Maestrini E et al. (2014) Maternally inherited genetic variants of CADPS2 are present in autism spectrum disorders and intellectual disability patients. EMBO Mol Med 6:795–809. CrossRef Medline

Brunk I, Blex C, Rachakonda S, Höltje M, Winter S, Pahner I, Walther DJ, Ahnert-Hilger G (2006) The first luminal domain of vesicular monoamine transporters mediates G-protein-dependent regulation of transmitter uptake. J Biol Chem 281:33373–33385. CrossRef Medline

Brunk I, Blex C, Speidel D, Brose N, Ahnert-Hilger G (2009) Ca2+-dependent activator proteins of secretion promote vesicular monoamine uptake. J Biol Chem 284:1050–1056. CrossRef Medline

Bruns D, Riedel D, Klingauf J, Jahn R (2000) Quantal release of serotonin. Neuron 28:205–220. CrossRef Medline

Daily NJ, Boswell KL, James DJ, Martin TF (2010) Novel interactions of CAPS (Ca^{2+}-dependent activator protein for secretion) with the three neuronal SNARE proteins required for vesicle fusion. J Biol Chem 285:35320–35329. CrossRef Medline

Eckenstaler R, Lessmann V, Brigadski T (2016) CAPS1 effects on intragranular pH and regulation of BDNF release from secretory granules in hippocampal neurons. J Cell Sci 129:1378–1390. CrossRef Medline

Finnegan JM, Pihel K, Cahill PS, Huang L, Zerby SE, Ewing AG, Kennedy RT, Wightman RM (1996) Vesicular quantal size measured by amperometry at chromaffin, mast, pheochromocytoma, and pancreatic beta-cells. J Neurochem 66:1914–1923. Medline

Forgac M (1989) Structure and function of vacuolar class of ATP-driven proton pumps. Physiol Rev 69:765–796. CrossRef Medline

Fujita Y, Xu A, Xie L, Arunachalam L, Chou TC, Jiang T, Chiew SK, Kourtesis J, Wang L, Gaisano HY, Sugita S (2007) Ca2+-dependent activator protein for secretion 1 is critical for constitutive and regulated exocytosis but not for loading of transmitters into dense core vesicles. J Biol Chem 282:21392–21403. CrossRef Medline

Gong LW, Hafez I, Alvarez de Toledo G, Lindau M (2003) Secretory vesicles membrane area is regulated in tandem with quantal size in chromaffin cells. J Neurosci 23:7917–7921. CrossRef Medline

Grabowski PAP, Bello AF, Rodrigues DL, Forbeci MJ, Motter V, Raskin S (2017) Deletion involving the 7q31–32 band at the CADPS2 gene locus in a patient with autism spectrum disorder and recurrent psychotic syndrome triggered by stress. Case Rep Psychiatry 2017:4254152. CrossRef Medline

Griesbeck O, Baird GS, Campbell RE, Zacharias DA, Tsien RY (2001) Reducing the environmental sensitivity of yellow fluorescent protein: mechanism and applications. J Biol Chem 276:29188–29194. CrossRef Medline

Hammarlund M, Watanabe S, Schuske K, Jorgensen EM (2008) CAPS and syntaxin dock dense core vesicles to the plasma membrane in neurons. J Cell Biol 180:483–491. CrossRef Medline

Henry JP, Sagné C, Bedet C, Gasnier B (1998) The vesicular monoamine transporter: from chromaffin granule to brain. Neurochem Int 32:227–246. CrossRef Medline

James DJ, Kowalchyk J, Daily N, Petrie M, Martin TF (2009) CAPS drives trans-SNARE complex formation and membrane fusion through syntaxin interactions. Proc Natl Acad Sci U S A 106:17308–17313. CrossRef Medline

James DJ, Khodthong C, Kowalchyk JA, Martin TF (2010) Phosphatidylinositol 4,5-bisphosphate regulation of SNARE function in membrane fusion mediated by CAPS. Adv Enzyme Regul 50:62–70. CrossRef Medline

Jockusch WJ, Speidel D, Sigler A, Sørensen JB, Varoqueaux F, Rhee JS, Brose N (2007) CAPS-1 and CAPS-2 are essential synaptic vesicle priming proteins. Cell 131:796–808. CrossRef Medline

Johnson RG Jr (1988) Accumulation of biological amines into chromaffin granules: a model for hormone and neurotransmitter transport. Physiol Rev 68:232–307. CrossRef Medline

Kabachinski G, Yamaga M, Kielar-Grevstad DM, Bruinsma S, Martin TF (2014) CAPS and Munc13 utilize distinct PIP2-linked mechanisms to promote vesicle exocytosis. Mol Biol Cell 25:508–521. CrossRef Medline

Kabachinski G, Kielar-Grevstad DM, Zhang X, James DJ, Martin TF (2016) Resident CAPS on dense-core vesicles docks and primes vesicles for fusion. Mol Biol Cell 27:654–668. CrossRef Medline

Khodthong C, Kabachinski G, James DJ, Martin TF (2011) Munc13 homology domain-1 in CAPS/UNC31 mediates SNARE binding required for priming vesicle exocytosis. Cell Metab 14:254–263. CrossRef Medline

Lin XG, Ming M, Chen MR, Niu WP, Zhang YD, Liu B, Jiu YM, Yu JW, Xu T, Wu ZX (2010) UNC-31/CAPS docks and primes dense core vesicles in C. elegans neurons. Biochem Biophys Res Commun 397:526–531. CrossRef Medline

Liu T, Xue R, Huang X, Zhang D, Dong L, Wu H, Shen X (2011) Proteomic profiling of hepatitis B virus-related hepatocellular carcinoma with magnetic bead-based matrix-assisted laser desorption/ionization time-of-flight mass spectrometry. Acta Biochim Biophys Sin (Shanghai) 43:542–550. CrossRef Medline

Liu Y, Schirra C, Stevens DR, Matti U, Speidel D, Hof D, Bruns D, Brose N, Rettig J (2008) CAPS facilitates filling of the rapidly releasable pool of large dense-core vesicles. J Neurosci 28:5594–5601. CrossRef Medline

Liu Y, Schirra C, Edelmann L, Matti U, Rhee J, Hof D, Bruns D, Brose N, Rieger H, Stevens DR, Rettig J (2010) Two distinct secretory vesicle-priming steps in adrenal chromaffin cells. J Cell Biol 190:1067–1077. CrossRef Medline

Machado JD, Díaz-Vera J, Domínguez N, Alvarez CM, Pardo MR, Borges R (2010) Chromogranins A and B as regulators of vesicle cargo and exocytosis. Cell Mol Neurobiol 30:1181–1187. CrossRef Medline

Matti U, Pattu V, Halimani M, Schirra C, Krause E, Liu Y, Weins L, Chang HF, Guzman R, Olausson J, Freichel M, Schmitz F, Pasche M, Becherer U, Bruns D, Rettig J (2013) Synaptobrevin2 is the v-SNARE required for cytotoxic T-lymphocyte lytic granule fusion. Nat Commun 4:1439. CrossRef Medline

Nguyen Truong CQ, Nestvogel D, Ratai O, Schirra C, Stevens DR, Brose N, Rhee J, Rettig J (2014) Secretory vesicle priming by CAPS is independent of its SNARE-binding MUN domain. Cell Rep 9:902–909. CrossRef Medline

Obergasteiger J, Überbacher C, Pramstaller PP, Hicks AA, Corti C, Volta M (2017) CADPS2 gene expression is oppositely regulated by LRRK2 and alpha-synuclein. Biochem Biophys Res Commun 490:876–881. CrossRef Medline

Sadakata T, Washida M, Furuichi T (2007a) Alternative splicing variations in mouse CAPS2: differential expression and functional properties of splicing variants. BMC Neurosci 8:25. CrossRef Medline

Sadakata T, Washida M, Iwayama Y, Shoji S, Sato Y, Ohkura T, Katoh-Semba R, Nakajima M, Sekine Y, Tanaka M, Nakamura K, Iwata Y, Tsuchiya KJ, Mori N, Detera-Wadleigh SD, Ichikawa H, Itohara S, Yoshikawa T, Furuichi T (2007b) Autistic-like phenotypes in Cadps2-knockout mice and aberrant CADPS2 splicing in autistic patients. J Clin Invest 117:931–943. CrossRef Medline

Sadakata T, Shinoda Y, Oka M, Sekine Y, Furuichi T (2013) Autistic-like behavioral phenotypes in a mouse model with copy number variation of the CAPS2/CADPS2 gene. FEBS Lett 587:54–59. CrossRef Medline

Speese S, Petrie M, Schuske K, Ailion M, Ann K, Iwasaki K, Jorgensen EM, Martin TF (2007) UNC-31 (CAPS) is required for dense-core vesicle but not synaptic vesicle exocytosis in Caenorhabditis elegans. J Neurosci 27:6150–6162. CrossRef Medline

Speidel D, Bruederle CE, Enk C, Voets T, Varoqueaux F, Reim K, Becherer U, Fornai F, Ruggieri S, Holighaus Y, Weihe E, Bruns D, Brose N, Rettig J (2005) CAPS1 regulates catecholamine loading of large dense-core vesicles. Neuron 46:75–88. CrossRef Medline

Stevens DR, Rettig J (2009) The Ca(2+)-dependent activator protein for secretion CAPS: do I dock or do I prime? Mol Neurobiol 39:62–72. CrossRef Medline

Tabares L, Alés E, Lindau M, Alvarez de Toledo G (2001) Exocytosis of catecholamine (CA)-containing and CA-free granules in chromaffin cells. J Biol Chem 276:39974–39979. CrossRef Medline

Vélez JI, Chandrasekharappa SC, Henao E, Martinez AF, Harper U, Jones M, Solomon BD, Lopez L, Garcia G, Aguirre-Acevedo DC, Acosta-Baena N, Correa JC, Lopera-Gomez CM, Jaramillo-Elorza MC, Rivera D, Kosik KS, Schork NJ, Swanson JM, Lopera F, Arcos-Burgos M (2013) Pooling/bootstrap-based GWAS (pbGWAS) identifies new loci modifying the age of onset in PSEN1 p.Glu280Ala Alzheimer's disease. Mol Psychiatry 18:568–575. CrossRef Medline

Walent JH, Porter BW, Martin TF (1992) A novel 145 kd brain cytosolic protein reconstitutes Ca^{2+}-regulated secretion in permeable neuroendocrine cells. Cell 70:765–775. CrossRef Medline

Wightman RM, Jankowski JA, Kennedy RT, Kawagoe KT, Schroeder TJ, Leszczyszyn DJ, Near JA, Diliberto EJ Jr, Viveros OH (1991) Temporally resolved catecholamine spikes correspond to single vesicle release from individual chromaffin cells. Proc Natl Acad Sci U S A 88:10754–10758. CrossRef Medline

Xue R, Tang W, Dong P, Weng S, Ma L, Chen S, Liu T, Shen X, Huang X, Zhang S, Dong L (2016) CAPS1 negatively regulates hepatocellular carcinoma development through alteration of exocytosis-associated tumor microenvironment. Int J Mol Sci 17 pii: E1626. CrossRef Medline

Zerbino DR, Achuthan P, Akanni W, Amode MR, Barrell D, Bhai J, Billis K, Cummins C, Gall A, Girón CG, Gil L, Gordon L, Haggerty L, Haskell E, Hourlier T, Izuogu OG, Janacek SH, Juettemann T, To JK, Laird MR et al. (2018) Ensembl 2018. Nucleic Acids Res 46:D754–D761. CrossRef Medline